

## GRAPHENE OXIDE/NANOCRYSTALLINE CELLULOSE COMPOSITE: A FACILE PHASE MODULATOR

Irene J. Ng'etich <sup>a</sup>, Elijah Mwangi <sup>b</sup>, Moses A. Ollengo <sup>a</sup>

<sup>a</sup> Dedan Kimathi University of Technology Nyeri, Kenya.

<sup>b</sup> University of Nairobi

### Abstract

In the past few years, graphene and graphene-based materials have received enormous interest from the scientific community due to their extraordinary mechanical, electronic, optical and electrochemical properties. The success of graphene applications highly motivates the exploration of other applications such as in designing of antennas, phase modulation, as a frequency multiplier, design of graphene-based Field Effect Transistors, its use as an electrode in batteries and as a supercapacitor. In this paper, we present the Graphene Oxide/ Nanocrystalline cellulose (GO/NCC) composite material experimental phase modulation investigation. The modulator produced a  $0.2\pi^c$  phase shift and the temporal profile obtained. The insertion loss at an ideal voltage of 2V and the extinction ratio was determined to be 15.17 dB at 25MHz and 12.22 dB respectively. The  $0.2\pi^c$  phase shift demonstrated by GO/NCC implies that it can be used in phase shift keying, specifically, in Off-set quadrature phase-shift keying modulation where a phase change of not greater than  $\frac{\pi}{2}$  radians at a time is required.

**Keywords:** Phase modulation, Insertion loss, Extinction ratio, Modulation index, Graphene Oxide/Nanocrystalline Cellulose (GO/NCC).

### I. Introduction

Phase modulation, an angle modulation technique, is the process of varying the phase of the carrier signal linearly with the message signal. This technique is very critical and has a wide range of applications in digital communication. Apart from it being widely used for transmitting radio waves and being an integral part of many digital transmission coding schemes that underlie a wide range of technologies like Wi-Fi, GSM and satellite television, phase modulation also finds application in photonic systems such as in Fiber-optic sensors and gyroscopes, integrated-optics sensors, or high-performance photonic integrated circuits[1]. Such a photonic system can be integrated as the core part of some specific applications like biosensors, 5G advanced optical communication devices, gyroscopes, or high-performance computation devices[1].

Others include in military electromagnetic warfare applications[2], in Polar and out-phasing transmitters[3] and improvement of ultrasonic imaging in aluminum plates[4] among various other applications.

In engineering, figures of merit are the key parameters that are often defined for particular materials or devices in order to determine their relative utility for an

application[5]. This also enables a comparison to be done on the material or device that has been fabricated against those previously fabricated for the same application. The key phase modulator parameters include: extinction ratio, insertion loss, modulation index and the modulation efficiency.

The Phase modulation index describes the peak phase difference between the modulated and unmodulated signal, given as  $h$ :

$$h = \Delta\theta \quad (i)$$

The insertion loss (IL) defines the loss or gain that is apparent upon inserting the network or device to be measured between a given source and a given receiver [6, 7]. It is given by:

$$\text{Insertion Loss (IL)} = 10\log_{10}(P_{in}/P_{out}), \quad (ii)$$

where  $P_{in}$  is power incident to the modulator, and  $P_R$  is the power transmitted from the modulator.

On the other hand, the extinction ratio gives the ratio of optical power when a one is transmitted versus when a zero is transmitted[8], given by:

$$\text{Extinction Ratio (ER)} = P_1/P_0 \quad (iii)$$

where  $P_1$  is the optical power level generated when the light source is on, and  $P_0$  is the power level generated when the light source is off.

These key parameters have been determined for the conventional phase modulators such as the Silicon-based phase modulators[9-12] and Lithium niobate ( $\text{LiNbO}_3$ ) phase modulator[13, 14] among others.

However, most of the above-mentioned modulators suffer from low modulation efficiency, large footprint, substantial temperature sensitivities, narrow operating bandwidth, and high insertion loss[15]. To be able to mitigate those limitations, a modulator with ultra-compact device footprint, small insertion loss, low energy consumption, ultrafast response, high modulation speed, broad operation bandwidth, and acceptable thermal tolerance is highly desirable[15].

Graphene[16] features unique properties such as strong coupling with light, gate-variable optical conductivity, extraordinary thermal conductivity in the range of 3000-5300W/mK[17], and ultrahigh saturable absorption[18], which show great potential applications in optical modulators.

A.Wirth-Lima et al.[19] presented Graphene-based Binary Phase-shift keying (BPSK) and Quadrature Phase Shift Keying (QPSK) modulators which could operate in the range from the Tera-Hertz up-to the infrared. These devices were noted to have huge

advantages over the Silicon Mach-Zehnder optical modulators (MZMs) with lateral PN-junction rib-waveguide phase shifters such as having only one waveguide and a much simpler application system of the modulator signal (gate voltage) than in silicon MZMs. A series of theoretical investigations and experimental demonstrations of graphene-based modulators have been extensively researched [20-28].

In this paper, we present a Graphene Oxide/Nanocrystalline Cellulose (GO/NCC) Phase modulator that offers huge advantages as compared to the silicon based MZMs such as having a much simpler design, greater efficiency and is cheaper. The phase shift, temporal profile as well as the key figures of merit that include the modulation index, extinction ratio and insertion loss is experimentally determined.

## II. Materials and Methods

### 1. Synthesis of Graphene Oxide/Nanocrystalline Cellulose Composite material (GO/NCC)

The NCC was prepared from dissolving pulp, obtained from a hard wood source, by means of hydrolysis with sulfuric acid (65% m/m). A mass of 5 g of dissolving pulp was mixed with 100 ml of sulfuric acid aqueous solution, and the mixture was stirred vigorously (700 PM) at 64°C for 1 hour. The mixture was diluted 10-fold with deionized water to stop the hydrolysis reaction and the diluted mixture was then centrifuged at 9000 RPM on a Hettich Zentrifugen, Universal 320 R, centrifuge, for 15 min to concentrate the cellulose and remove excess aqueous acid. A precipitated solid material was rinsed with distilled water and centrifuged again; this process was repeated 3 times. The material was subsequently dialyzed in Sigma-Aldrich dialysis sacks, against deionized water for one week until a pH of 7 was reached. The dialyzed nanocellulose was sonicated in an ultrasonic bath (UP400S 400W, Hielscher Co., Germany), for 5min under cooling in a bath at 75% output and 0.7 cycles to obtain a NCC colloidal solution.

Graphene Oxide (GO) was prepared using a modified Hummer's method[29]. In this synthesis, Graphite was first mixed with Sulphuric acid in a reaction vessel. While keeping the mixture in an ice water bath, Sodium Nitrate was added. Potassium permanganate (KMnO<sub>4</sub>) was then added to the mixture and Graphene Oxide obtained from this reaction as the temperature was maintained below 15°C. The water bath was removed and the reaction temperature was then increased to 50°C. Hydrogen Peroxide was added, followed by several cycles of washing with double deionized water (DI) until the filtrate reached a neutral pH. The concentration of the synthesized GO was determined by accurately weighing duplicate aliquots. The aliquots were dried overnight in an oven set at 50°C. The aliquots were reweighed and the concentration was expressed as the average mass of the duplicate aliquots after drying over average mass before drying. This was then followed by NCC/GO composite synthesis.

The NCC/GO composite was then prepared by dispersing the Graphene Oxide synthesized in an ultrasonic water bath treatment as the NCC was added. The resultant composite solution was transferred to a petri-dish to allow for slow evaporation of water in a controlled dust-free environment and dried in order to obtain the composite film.

## 2. Determination of the key phase modulator parameters

The temporal profile and the phase change effected by the GO/NCC Phase modulator were determined by connecting it to the signal generator and the output obtained from the Digital oscilloscope.

To determine the Insertion Loss, the RF Signal generator was connected to the Graphene Oxide/Nanocrystalline Cellulose phase modulator material and the output connected to the spectrum analyzer. The power input ( $P_{in}$ ) and power output from the modulator ( $P_{out}$ ) was obtained from the spectrum analyzer as the voltage and frequency were varied.

The extinction ratio was determined by connecting the GO/NCC modulator material to the Optical source of the Scientech Optical communication system and the output power when the optical source was switched on and off obtained from the network analyzer.

## III. Results and Discussion

A 3D image of the Graphene Oxide/Nanocrystalline Cellulose sample synthesized was obtained by using the Zeiss Axio Zoom.V16 Camera Microscope and the Scanning Electron Microscope (SEM). The GO/NCC sample film produced had a thickness of  $49.41\mu\text{m}$ . When a signal from the signal generator was passed through the sample, a phase shift  $0.2\pi^\circ$  was realized. The temporal profile was obtained from the CRO.

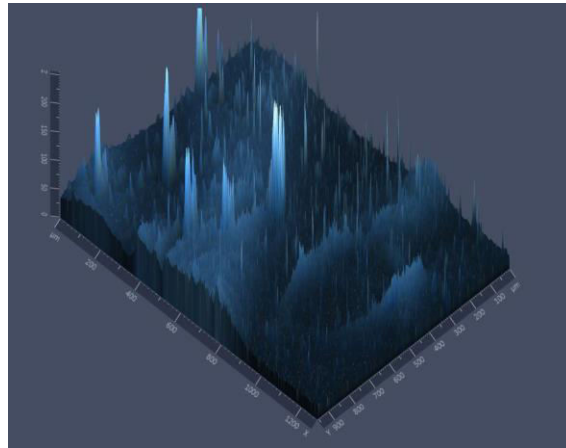


**Fig 1:** 3D image of the GO/NCC sample film synthesized having a thickness of  $49.41\mu\text{m}$  with rod-like protrusions as observed under the Zeiss Axio Zoom.V16 Camera Microscope.

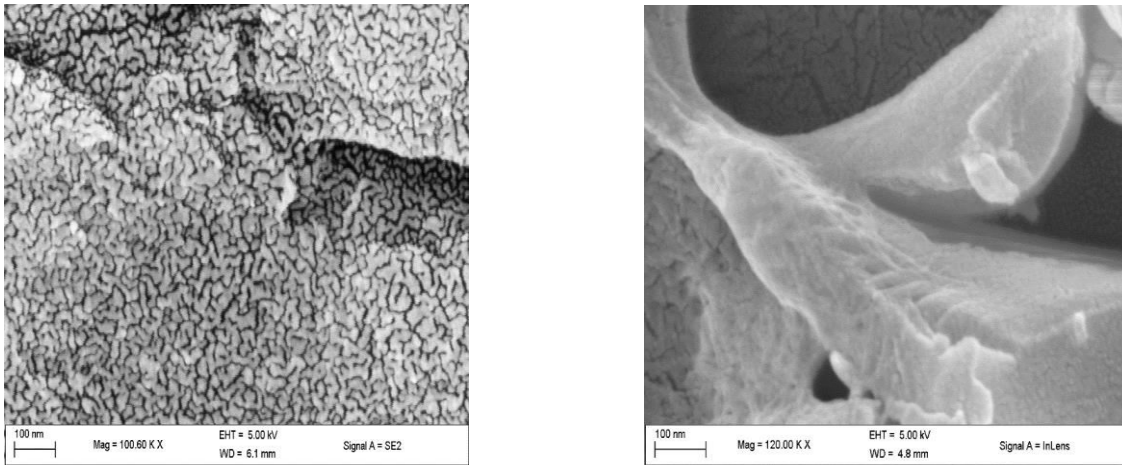


**Fig 2:** SEM IMAGE of (a) GO and (b) NCC.

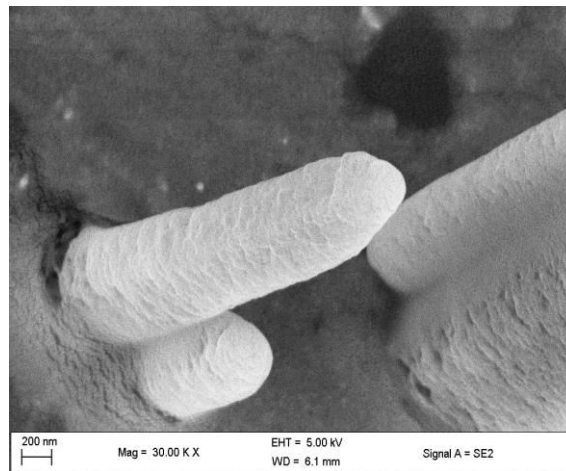


**Fig 3:** SEM IMAGE of GO/NCC

The high number of OH groups on the surface of nanocrystalline cellulose is likely to favor hydrogen bonding. In this regard, the hydrogen bonding becomes the binding force between a nanocrystalline cellulose film sandwiched between two graphene oxide sheets, thereby forming a composite film. The nanocrystalline cellulose forms a thin layer of rods (as shown in Fig 1 and Fig 3) in between the graphene oxide monolayers since it assumes nematic order in colloidal dispersions occasioned by whisker entanglements. The interaction between the chiral surfaces and the twisted morphology of nanocrystalline cellulose and the overlaying graphene oxide monolayer provides an avenue for response to external applied electric or magnetic fields.

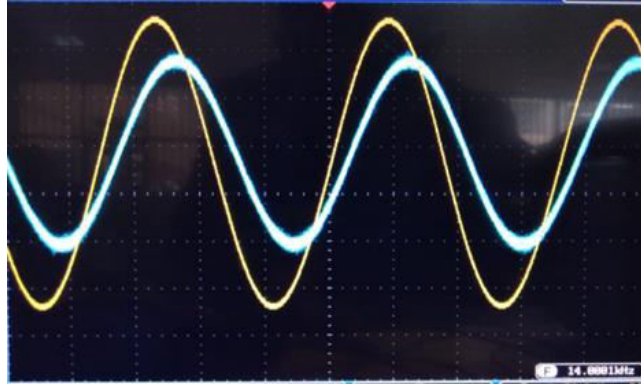


**Fig 4:** Temporal Profile of the GO/NCC modulator exhibiting the phase shift.

The insertion loss experiment was performed on the GO/NCC as the voltage was varied from 0V to 20V and the graph obtained is as shown in Fig. 5.

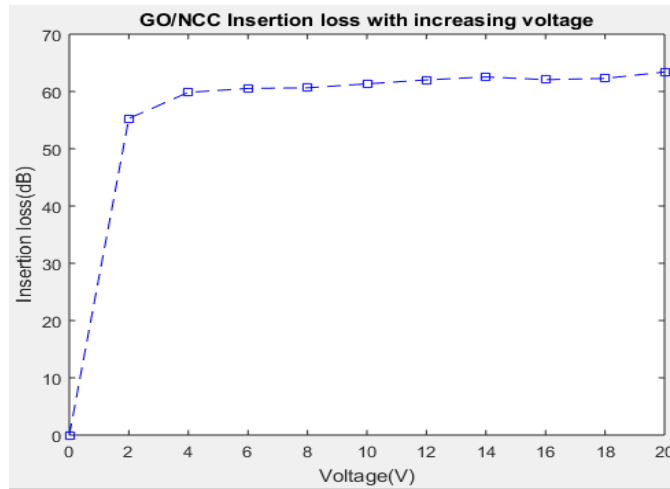


**Fig 5:** A graph of the GO/NCC modulator Insertion loss with increasing voltage (0 to 20v).

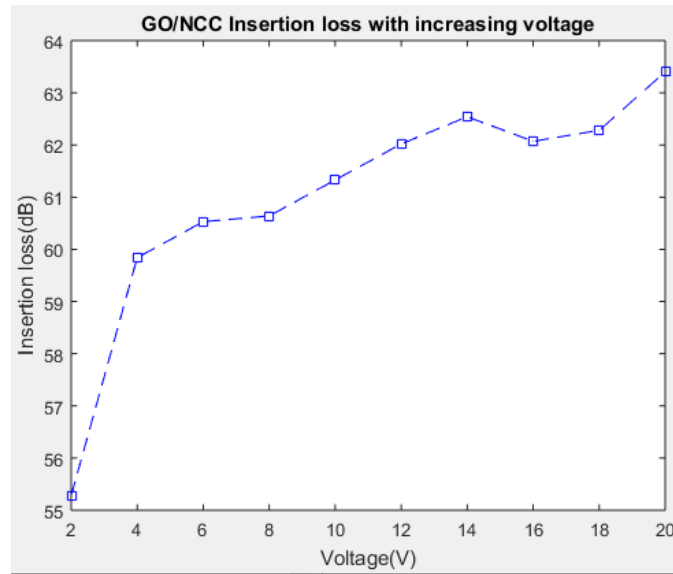


**Fig 6:** A graph of the GO/NCC modulator Insertion loss with increasing voltage (2 to 20V).

The Graphene Oxide structure consists of the  $sp^2$  carbons that have a higher electronegativity value of carbon, while the  $sp^3$  carbons, by virtue of them being hooked to oxygen, are devoid of electrons. Hence, they act as holes. Oxygen is more electronegative than carbon, therefore, carbon will appear positive. This essentially creates a hole within the structure of Graphene Oxide.

The NCC held in between the Graphene Oxide is presumed to be a perfect insulator. However, due to the presence of oxygen groups, it can easily promote coupling. This therefore explains the phenomenon that is observed between 0 to 2 V where there is an upsurge of the energy consumed due to a higher combination, that is, the electron-electron and electron-phonon coupling.

From 2V onwards to 20V, there is a gradual increase in energy consumed since it is now majorly driven by the electron – phonon couplings. As a higher voltage is applied, variations are observed that is attributed to the changes in the structure of the GO/NCC.

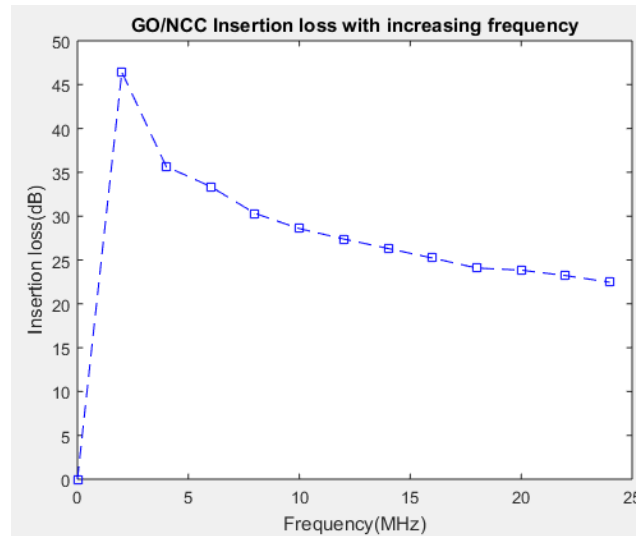


**Fig 7:** Graph of GO/NCC Insertion loss vs frequency.

Fig. 7 shows the graph of the GO/NCC insertion loss with increasing frequency. Initially, the insertion loss increased before significantly decreasing upon increase of frequency. This confirms the work done by W. Kim et al. on radio frequency characteristics of graphene oxide where the impedance and resistance of graphene sheets drastically decrease as frequency increases. Consequently, the insertion loss also decreases. This confirms graphene oxide has a high potential for use at gigahertz ranges.

Normally, a driving voltage of above 5V is not compatible with the microelectronic integrated circuits since it is very difficult for CMOS chips to supply such a high voltage at a high frequency. Also, a higher voltage (above 5V) results in the widening of the noise margin and this is undesirable. Low voltage also means low power consumption and less heat dissipation problems. Therefore, at an ideal voltage of 2V, an insertion loss of 15.17dB at 25MHz was obtained.

Further research can be done to lower the GO/NCC Phase modulator Insertion Loss to nearly 0dB hence improving its performance.

An extinction ratio (ER) of 12.22dB was obtained for the GO/NCC modulator. The ER is an important metric since it has an impact on a device's performance. It should be ideally larger than 10dB (preferably 10-15dB). As the extinction ratio improves, the Bit-error ratio improves, reducing the number of errors and the amount of error correction required. A poorer value of ER increases the power penalty and worsens the Bit Error Ratio.

#### IV. Conclusion

In conclusion, the GO/NCC Phase Modulator has been characterized using the following key parameters: The modulator produced a  $0.2\pi$  radians phase shift and the temporal profile obtained. The  $0.2\pi$  modulation index demonstrated by GO/NCC implies that it can be used in phase shift keying, specifically, in Off-set quadrature phase-shift keying

modulation where a phase change of not greater than  $\frac{\pi}{2}$  radians at a time is required. The insertion loss at an ideal voltage of 2V and the extinction ratio was determined to be 15.17 dB and 12.22 respectively. Ideally, the insertion loss and the extinction ratio should generally be lower than a few dB and larger than 10dB respectively for a modulator.

## References

- [1] R. Menéndez, "Modulation in Electronics and Telecommunications - Optical Phase-Modulation Techniques," vol. 10.5772/intechopen.75319, 2019, doi: 10.5772/intechopen.90343.
- [2] F. Urick, S. Devgan, and J. McKinney, "[IEEE 2007 IEEE Avionics, Fiber-Optics and Photonics Technology Conference - Victoria, BC, Canada (2007.10.2-2007.10.5)] 2007 IEEE Avionics, Fiber-Optics and Photonics Technology Conference - Analog Phase Modulation for Avionics Applications," pp. 7-8, 2007, doi: 10.1109/avfop.2007.4365721.
- [3] P. Nidhi, and S. Pamarti, "Open-Loop Wide-Bandwidth Phase Modulation Techniques," *Journal of Electrical and Computer Engineering*, vol. 2011, pp. 1-12, 2011, doi: 10.1155/2011/507381.
- [4] R. Tischer, R. Higuti, and C. Kitano, "Improving ultrasonic imaging of aluminum plates using phase modulation," *Journal of Integrated Circuits and Systems* vol. 15, no. 3, pp. 1-5, 2020, doi: 10.29292/jics.v15i3.191
- [5] A. Olivieri, "Practical Three-Way Calibration || Analytical Figures of Merit," Elsevier, pp. 93-107, 2014, doi: 10.1016/B978-0-12-410408-2.00006-5.
- [6] W. Valkenburg, "Reference Data for Engineers - Radio, Electronics, Computer, etc, 9 ed. Newnes", 2002.
- [7] M. Ams, "Laser Growth and Processing of Photonic Devices - Femtosecond-laser-induced refractive index modifications for photonic device processing," pp. 305-332, 2012, doi: 10.1533/9780857096227.3.305.
- [8] C. DeCusatis, "Handbook of Fiber Optic Data Communication 4ed." Elsevier, 2014.
- [9] H. Mahrous, and Afifi, Ahmed, "Design of compact, high-speed and low-loss silicon-on-silica electro-optic modulators," *Semiconductor Science and Technology*, 2020, doi: 10.1088/1361-6641/ab9d09.
- [10] C. Kieninger, H. Zwickel, Y. Kutuvantavida, J. Kemal, C. Eschenbaum, D. Elder et al., "Silicon-organic hybrid (SOH) Mach-Zehnder modulators for 100 GBd PAM4 signaling with sub-1 dB phase-shifter loss " *Optics Express*, vol. 28, no. 17, pp. 24693-24707, 2020, doi: 10.1364/OE.390315.
- [11] X. Oberhammer, "Micromachined Subterahertz Waveguide-Integrated Phase Shifter Utilizing Supermode Propagation," *IEEE Transactions on Microwave Theory and Techniques ( Early Access )*, 2021, doi: 10.1109/TMTT.2021.3076079.
- [12] J. Zhang, S. Qin, M. Cheng, K. Wang, L. Kai, and J. Sun, "Asymmetric Ge/SiGe coupled quantum well modulators," *Nanophotonics*, vol. 10, no. 6, pp. 1765-1773, 2021, doi: 10.1515/nanoph-2021-0007.
- [13] C. Kharel, K. Luke, L. He, and M. Zhang "Breaking voltage–bandwidth limits in integrated lithium niobate modulators using micro-structured electrodes," *Optica*, vol. 8, no. 3, pp. 357-363, 2021, doi: 10.1364/OPTICA.416155.
- [14] A. Choudhary, A. Singh, D. Chaudhary, and S. Kumarab, "Implementation of highly optimized optical all logic gates on a single chip using Ti-diffused lithium-niobate for high-speed processing in combinational circuits," *Microelectronics Journal*, vol. 111, 2021, doi: 10.1016/j.mejo.2021.105048.

- [15] X. Jian et al., "Design of graphene-based polarization-insensitive optical modulator," *Nanophotonics*, vol. 7, no. 3, 2018, doi: 10.1515/nanoph-2017-0088.
- [16] A. Geim et al., "The rise of graphene," *Nature Materials* vol. 6, no. 3, p. 183—191, 2007, doi: 10.1038/nmat1849.
- [17] S. Mbambo, T. Kahmliche, M. Moodley, K. Kaviyarasu, I. Madiba et al., "Remarkable thermal conductivity enhancement in Ag decorated graphene nanocomposites based nanofluid by laser liquid solid interaction in ethylene glycol," *Scientific Reports*, vol. 10, no. 1, 2020, doi: 10.1038/841598-020-67418-3.
- [18] H. Qi, H. Cui, Y. Huang, Q. Ning, M. Liu et al. , "Graphene-deposited microfiber photonic device for ultrahigh-repetition rate pulse generation in a fiber laser," *Optics Express*, vol. 23, no. 14, 2015, doi: 10.1364/OE.23.017720.
- [19] W. Wirth-Lima, "Graphene-based BPSK and QPSK modulators working at a very high bit rate (up Tbps range)," *Optical and Quantum Electronics*, 2021, doi: 10.1007/s11082-021-02928-6.
- [20] Z. Lu et al., "Nanoscale electro-optic modulators based on graphene-slot waveguides," *Journal of the Optical Society of America B*, vol. 29, no. 6, p. 1490, 2012, doi: 10.1364/josab.29.001490.
- [21] L. Ting; H. Ran; Q. Chen; X. Chao; Y. Hui; X. Yang et al., "Low-chirp high-extinction-ratio modulator based on graphene–silicon waveguide," *Optics letters*, vol. 38, no. 14, p. 2512, 2013, doi: 10.1364/ol.38.002512.
- [22] S. Koesteret al., "High-speed waveguide-coupled graphene-on-graphene optical modulators," *Applied Physics Letters*, vol. 100, no. 17, p. 171107, 2012, doi: 10.1063/1.4704663.
- [23] J. Goscinia, and T. Dawn, "Theoretical investigation of graphene-based photonic modulators," *Scientific Reports*, vol. 3, 2013, doi: 10.1038/srep01897.
- [24] C. Yichang, Y. Longzhi, Y. Jianyi, and J. Xiaoqing, "Characteristics of electrorefractive modulating based on graphene-oxide-silicon waveguide," *Optics Express*, vol. 20, no. 20, p. 22398, 2012, doi: 10.1364/OE.20.022398.
- [25] B. Rusen, Z. Mingda, J. Debdeep, L. Lei, and G. Huili, "Efficient terahertz electro-absorption modulation employing graphene plasmonic structures," *Applied Physics Letters*, vol. 101, no. 26, p. 261115, 2012, doi: 10.1063/1.4773374.
- [26] B. Rusen, M. Kelly, F. Tian, T. Kristof, H. Wan Sik, J. Debdeep et al., "Broadband graphene terahertz modulators enabled by intraband transitions," *Nature Communications*, vol. 3, p. 780, 2012, doi: 10.1038/ncomms1787.
- [27] C. Phare, Y. Ho, C. Jaime, and L. Michal, "Graphene electro-optic modulator with 30 GHz bandwidth," *Nature photonics*, vol. 9, no. 8, pp. 511-514, 2015, doi: 10.1038/nphoton.2015.122.
- [28] H. Yang, W. Yuan, and Z. Xiang "Athermal Broadband Graphene Optical Modulator with 35 GHz Speed," *ACS Photonics*, p. acsphotronics.6b00398, 2016, doi: 10.1021/acsphotronics.6b00398.
- [29] N. Zaaba, U. Hashim, S. Tan, L. Wei-Wen, and C. Voon, "Synthesis of graphene oxide using modified hummers method: solvent influence," *Procedia Engineering*, vol. 184, pp. 469-477, 2017, doi: 10.1016/j.proeng.2017.04.118.